A 130 point Nd:YAG Thomson scattering diagnostic on MAST[a)]

R. Scannell,[1,b)] M. J. Walsh,[1,c)] M. R. Dunstan,[1] J. Figueiredo,[1] G. Naylor,[1] T. O'Gorman,[1] S. Shibaev,[1] K. J. Gibson,[2] and H. Wilson[2]
[1]*EURATOM/CCFE Fusion Association, Culham Science Centre, Abingdon, Oxon OX14 3DB, United Kingdom*
[2]*Department of Physics, University of York, Heslington, York YO10 5DD, United Kingdom*

(Presented 17 May 2010; received 14 May 2010; accepted 28 May 2010; published online 14 October 2010)

A Thomson scattering diagnostic designed to measure both edge and core physics has been implemented on MAST. The system uses eight Nd:YAG lasers, each with a repetition rate of 30 Hz. The relative and absolute timing of the lasers may be set arbitrarily to produce fast bursts of measurements to suit the time evolution of the physics being studied. The scattered light is collected at F/6 by a 100 kg six element lens system with an aperture stop of 290 mm. The collected light is then transferred to 130 polychromators by 130 independent fiber bundles. The data acquisition and processing are based on a distributed computer system of dual core processors embedded in 26 chassis. Each chassis is standalone and performs data acquisition and processing for five polychromators. This system allows data to be available quickly after the MAST shot and has potential for real-time operations. [doi:10.1063/1.3460628]

I. INTRODUCTION

A major upgrade to the existing core Nd:YAG Thomson scattering (TS) system on MAST has now been completed. The outline design for this upgrade system is described in Ref. 1. The implementation and first results from this system are discussed in this paper. The new system has greatly increased the temporal and spatial resolution with respect to the previous system.[2] A summary of the capabilities of the existing and upgraded systems is given in Table I. As well as the increase in resolution, the upgraded system has embedded computing for fast processing and flexible triggering to measure events and a laser alignment system to ensure that consistent calibration is maintained.

The installation of the upgraded diagnostic has had an impact on two existing TS systems installed on MAST. An edge system measuring at high resolution in the pedestal region[3] and a Ruby system[4] measuring in the plasma core. The edge system uses separate collection optics but has benefited from the additional lasers and higher laser energy. The Ruby TS system shares the core collection optics with the Nd:YAG system and has been adapted to operate with the larger lens installed in the upgrade. The modifications to the Ruby system, described in Ref. 5, increase the spatial resolution and allow double pulsing of the Ruby laser.

II. LASERS

Eight 1.6 J 30 Hz Nd:YAG lasers are now operational on MAST. Four of these lasers are modified from existing 50 Hz 1.0 J lasers and four additional lasers were obtained. In equispaced operation, the eight lasers are combined to provide 240 Hz measurements. However, the lasers are frequently operated in short bursts to obtain high time resolution[6] or in pairs to obtain high spatial resolution in the pedestal region.[7] The timing of the lasers is synchronized to the MAST clock. Hence, if the time of an event is known, the eight lasers may be set to fire at arbitrary time resolution about the event. Synchronization to the MAST clock is achieved by a Smart trigger unit.[8] The Smart trigger unit also allows the system to be operated using event triggering.

The eight lasers travel a 30 m beam path to the MAST vessel. The profile of the laser beams is controlled by two cylindrical lenses; a 4.5 m focusing lens then focuses the lasers close to a spot in the object plane of the optical fibers. The Nd:YAG lasers follow a path 14.5 mm above the vertical center of the MAST vessel, the Ruby laser follows a path 14.5 mm below as shown in Fig. 1. The size of the laser beam shown in this image has been obtained from burn patterns and represents $\sim \pm 2\sigma$ of the beam width. The height of a rectangular optical fiber bundle in the backplane is 2.02 mm. The image of this fiber end is magnified by a factor of 3.3 to 4.1 in the plasma dependent on the major radius. The fiber images are largest close to the center column where high radial resolution is obtained due to the near tangency of the laser beam to the plasma major radius. At the outboard and center of the plasma, the radial resolution obtained is similar to the scattering length due to the near radial path of the laser beam.

The laser beams impacts on a stainless steel beam dump consisting of narrow blades creating a surface at a steep angle to the direction of the laser beam propagation. The beam dump is located outside the vessel. The path to the ex-vessel dump contains baffles to minimize the reflection of light from the dump. The beam dump can be moved out of the laser path using a retractable drive to allow helium neon alignment laser beams through the vessel.

[a)]Contributed paper, published as part of the Proceedings of the 18th Topical Conference on High-Temperature Plasma Diagnostics, Wildwood, New Jersey, May 2010.
[b)]Electronic mail: rory.scannell@ccfe.ac.uk.
[c)]Present Address: ITER Organisation, Diagnostics Division, Cadarache, 13106 St. Paul-lez-Durance, France.

TABLE I. Comparison of upgrade and existing Nd:YAG systems.

	Pre-2009	Upgrade
Number of lasers	4	8
Repetition rate per laser (Hz)	50	30
Pulse energy (J)	1.0	1.6
Collection F/#	12	6
Spatial points	19	130
Scattering length (mm)	20–40	10

III. COLLECTION LENS

The upgrade system collects light at F/6 along an approximately 1.3 m viewing chord, collecting four times as much light as the previous core system, which collected along the same chord at F/12. The collection cell, shown in Fig. 2, consists of six individual lens elements correcting for chromatic aberration. Four of the lenses are fused silica; the remaining two lenses are flint and are made from RS52 and RS32 "*Pilkington radiation resistant*" material. The spatial smearing by the lens is small compared to the 10 mm size of the fiber bundles in the object plane. The radial resolution achieved was measured by back illuminating optical fiber bundles through the collection cell and was found to be below 11 mm across the plasma. Designing the collection cell using mirrors, as in Ref. 9, was also considered but eventually rejected due to the large optical surfaces required close to the MAST vessel. The collection lens views the plasma through a 380 mm diameter silica vacuum window. The window is protected from glow discharges and boronization between plasma pulses by a mechanical blade shutter system. The shutter system consists of six blades, which rotate into place as shown in Fig. 3.

The lens is designed to measure from 550–1100 nm, and transmission is expected to be greater than 80% above 600 nm. Each lens element has been coated to reduce reflections. The overall transmission of the collection lens has been tested using a red diode laser and found to be ~86%. These transmission losses are consistent with a reflection of ~1% per surface. Five broadband wiregrid polarizers of width 90 mm have been installed in front of the optical fibers to reduce randomly polarized plasma background light by a factor of two.

The alignment of the collection cell to the laser beam is achieved by measurements of Raman scattered light from nitrogen gas. It is possible to adjust the collection cell height vertically and obliquely by means of three nuts securing the collection cell to an optical bench at either side of the front of the collection cell and centrally at the back of the collection cell. The alignment was monitored by examining the radial intensity profiles of scattered signals and by monitoring relative intensity of signals as a function of time in vertically split fiber bundles.

The combined collection cell weighs ~100 kg, ~80 kg due to the lenses and the remainder due to the aluminum cell. The collection cell was assembled in an optical clean room and installed in the MAST area using a crane system. This allowed the cell to be carefully lowered into place with a high degree of precision.

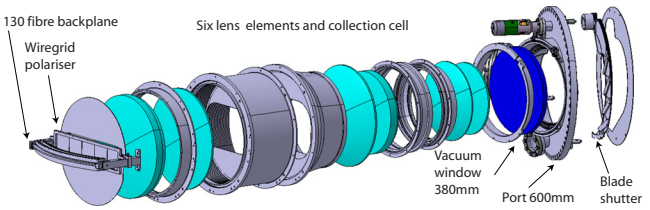

FIG. 2. (Color online) Components making up the combined collection lens and window.

IV. OPTICAL FIBERS

The collected light is relayed from the back of the collection lens to the spectrometer room along a 30 m path via 132 optical fiber bundles. Each fiber bundle consists of 130 individual strands of fiber of 210/230 μm diameter. At the collection cell end, the fibers in a single bundle are hexagonally close packed in a rectangle of 13×10, 13 along the direction of laser beam propagation and ten orthogonal to the direction of laser beam propagation. At the spectrometer end, the fibers form a circle of diameter 3 mm. The fibers at the circular end are randomized with respect to their position at the rectangular end as shown in Fig. 4. The 132 fiber bundles were inspected for dead fiber strands. This inspection revealed that 35 bundles had a single dead fiber, ten bundles had two dead fibers, and 87 fiber bundles had all 130 fiber strands intact.

The numerical aperture of the fibers falls off as a function of length. At 30 m, the fibers are calculated to have a numerical aperture of 0.275, which corresponds to an F number of 1.818. This F number is well matched to the image plane of the collection lens and the input of the spectrometer,

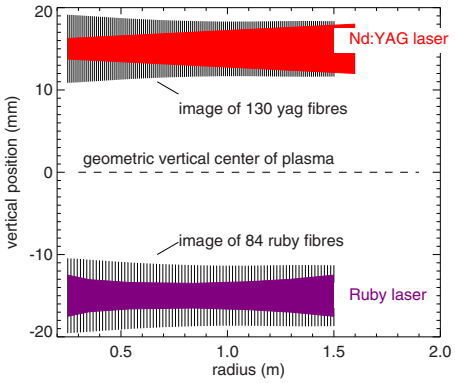

FIG. 1. (Color online) Size of Nd:YAG and Ruby laser beam waists and image of optical fibers in the plasma.

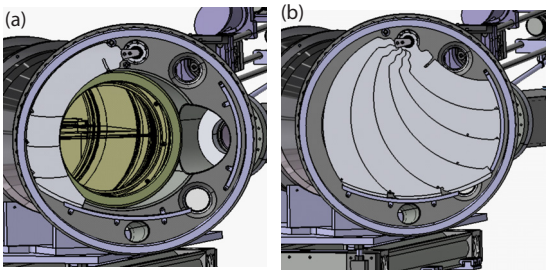

FIG. 3. (Color online) Rotating blade shutter in open and closed position used to protect the window.

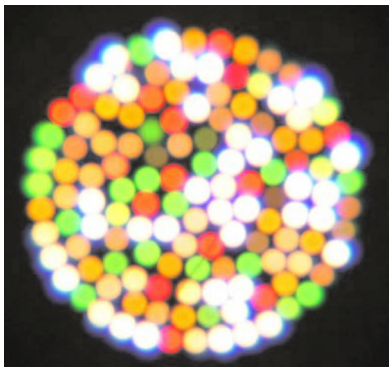

FIG. 4. (Color online) Image of circular fiber resulting from the illumination of four quarters of the rectangular end of the bundle with different colors. This illustrates the randomization of the fibers.

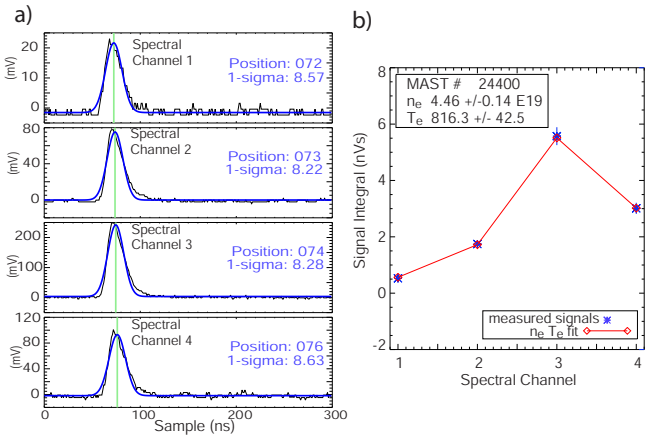

FIG. 5. (Color online) (a) Measured scattered signals overlaid with fits performed on the embedded computer system. (b) The spectral fit performed to the signal integrals to obtain temperature and density.

which both have F number of 1.75. The theoretical transmission of an optical fiber strand over a length of 30 m is greater than 90% from 700–1100 nm, with the exception of a small dip to ~88% at 900 nm due to the OH absorption peak. Low OH fibers were selected since these are expected to have a slightly higher transmission in the red part of the spectrum.

Two of the optical fiber bundles have two distinct groups of 65 fiber strands. One of the two groups follows a 45 m optical path, and the other follows a 30 m optical path. The two groups of strands are recombined at the collection lens end of the fiber, the top five rows and bottom five rows corresponding to the different optical path lengths. The strands from the two lengths of fibers are combined and randomized at the spectrometer end. The scattered pulse arrival time in the spectrometer allows for a vertical alignment measurement of the laser to be obtained as discussed in Ref. 10.

V. POLYCHROMATORS

125 new spectrometers were assembled for the upgrade system. Each spectrometer contains 23 lens elements, five mirrors and interference filters, and seven printed circuit boards. A modular approach to the assembly process resulted in an assembly time of 2 days per spectrometer. Five spectrometers from the existing core system were modified and incorporated into the upgrade diagnostic.

The spectrometer design is similar to that described in Refs. 1 and 3. Each spectrometer measures five different wavelength bands. The avalanche photodiode for each wavelength band requires the dc level and reverse bias voltage to be individually set. The temperature compensation of the APD (avalanche photodiode) gain was achieved by setting a temperature dependent feedback to the reverse bias voltage. The magnitude of the feedback required was found to vary with the wavelength band measured by the APD. As well as compensating the spectrometers to make them insensitive to temperature variation, as a further precaution, the spectrometer area is kept at an approximately constant temperature by air conditioning. The setting of variable resistors for dc level, reverse bias voltage, and temperature zero point for five channels of each spectrometer was performed using a LABVIEW program, which digitized all 15 signals simultaneously.

The duration of laser pulses is 7 ns full width at half maximum (FWHM). The measured scattered pulses are fitted as Gaussians and have mean 1-sigma of 5.5 ns corresponding to a FWHM of 13 ns. The broadening of the pulse shape is a combination of the APD detector response and amplifier response. The fast response of the detector causes a negative undershoot in the pulse shape. The amplifier circuit removes the undershoot at the expense of some pulse broadening. The removal of the undershoot allows the digitizer range to be used more effectively to predominantly measure positive signal. Measured scattered pulse shapes and Gaussians fitted to them are shown in Fig. 5.

VI. DATA ACQUISITION

Data acquisition is based on a 26 CPU distributed computer system. Each computer is embedded in a cPCI chassis unit housing either five or six ADC cards providing either 20 or 24 1 GSample/s ADC channels. Each chassis provides the digitizers for five spectrometers. This module of five spectrometers and a single chassis is replicated across nine cubicles. Eight cubicles contain three of these modules, and a final cubicle contains two of these modules and also the miscellaneous hardware, such as laser power measurements and triggering systems. The layout of the data acquisition system is shown in Fig. 6.

Due to the modular design, the scattered signal data collected from any spectrometer are read by a single computer. This allows for the real-time calculation of electron temperature and density (T_e and n_e) on that computer without communication to other computers over the network. The data processing from raw scattered signals to T_e and n_e may be divided into two steps. The first is the integration of the scattered signals. The second is the processing of these *integrals* to calculate T_e and n_e. The integration of the scattered signals is performed on the embedded computers to make use of the distributed processing power. The calculation of T_e and n_e from the integrals is performed centrally in the MAST processing loop since it also requires detailed calibration data, laser energy, and access to the slow sampled background light data. A sample of the fits to obtain the integrals and to obtain T_e and n_e from these integrals is shown in Fig. 5.

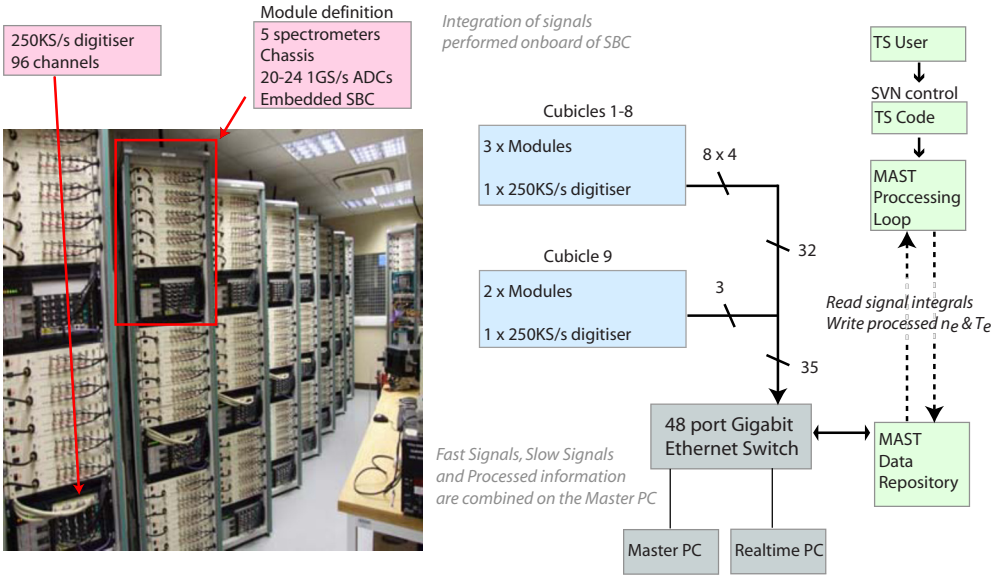

FIG. 6. (Color online) Image and flow diagram of assembled sectrometer and data acquisition system.

In addition to the centrally processed data, provisional values of T_e and n_e are determined onboard of the embedded computer. These onboard T_e and n_e are determined using a look up table. The lookup table is tabulated for each spectrometer using its spectral and Raman calibration. The table contains signal as a function of electron temperature for each channel at a plasma density of 10^{19} m^{-3}. The T_e and n_e data determined in this manner are available immediately after the MAST pulse and are available during the shot.[11] The more accurate T_e and n_e determined from central processing in the MAST loop are available several minutes after the pulse.

VII. RESULTS

The seven profiles shown in Fig. 7 illustrate a sawtooth crash. The lasers were fired with 20 μs separation between subsequent laser pulses. The first profile (red) shows a centrally peaked core temperature of maximum temperature 650 eV taken 100 μs before the collapse of the soft x-rays. The subsequent profiles show a region of elevated temperature surrounded by a strong gradient. This region of high temperature narrows as the sawtooth proceeds before the eventual expulsion of the hot core region. The final profile (dark green) taken 20 μs after the collapse of the soft x-rays shows a centrally flat temperature region of 500 eV over ~0.7 m. The hot particles from the core have been distributed outwards and the edges of the central flattened region of 500 eV extend beyond the $T_e > 500$ eV region before the sawtooth.

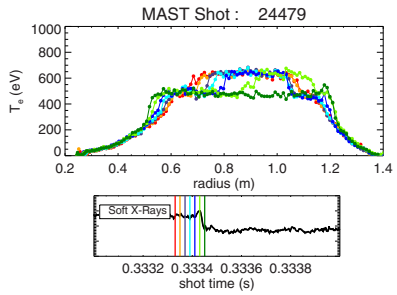

FIG. 7. (Color online) Plasma temperature profiles obtained during a sawtooth collapse where lasers are fired 20 μs apart.

ACKNOWLEDGMENTS

This work was funded partly by the United Kingdom Engineering and Physical Sciences Research Council under Grant No. P/G003955 and the European Communities under the Contract of Association between Euratom and CCFE. The views and opinions expressed herein do not necessarily reflect those of the European Commission. This work was carried out within the framework of the European Fusion Development Agreement. This work was also partly funded by the University of York and the Northern Way. The author would like to acknowledge the help of the very many people who contributed to this project in the MAST Team.

[1] R. Scannell, M. J. Walsh, P. G. Carolan, A. C. Darke, M. R. Dunstan, R. B. Huxford, G. McArdle, D. Morgan, G. Naylor, T. O'Gorman, S. Shibaev, N. Barratt, K. J. Gibson, G. J. Tallents, and H. R. Wilson, Rev. Sci. Instrum. **79**, 10E730 (2008).
[2] M. Walsh, E. Arends, P. G. Carolan, M. R. Dunstan, M. J. Forrest, S. K. Nielsen, and R. O'Gorman, Rev. Sci. Instrum. **74**, 1663 (2003).
[3] R. Scannell, M. Walsh, P. G. Carolan, N. J. Conway, A. C. Darke, M. R. Dunstan, D. Hare, and S. L. Prunty, Rev. Sci. Instrum. **77**, 10E510 (2006).
[4] M. Walsh, N. J. Conway, M. R. Dunstan, M. J. Forrest, and R. B. Huxford, Rev. Sci. Instrum. **1**, 70 (1999).
[5] T. O'Gorman, "Design and implementation of a full profile sub-cm Ruby based Thomson scattering system for MAST," Rev. Sci. Instrum. (to be published).
[6] R. Scannell, A. Kirk, N. Ben Ayed, P. G. Carolan, G. Cunningham, J. McCone, S. L. Prunty, and M. J. Walsh, Plasma Phys. Controlled Fusion **49**, 1431 (2007).
[7] H. Meyer, C. Bunting, P. G. Carolan, N. J. Conway, M. R. Dunstan, A. Kirk, R. Scannell, D. Temple, M. Walsh, and MAST and NBI Teams, J. Phys.: Conf. Ser. **123**, 012005 (2008).
[8] G. Naylor, Rev. Sci. Instrum. **81**, 10E110 (2010).
[9] R. Pasqualotto, P. Nielsen, C. Gowers, M. Beurskens, M. Kempenaars, T. Carlstrom, and D. Johnson, Rev. Sci. Instrum. **75**, 3891 (2004).
[10] J. Figueiredo, G. Naylor, M. Walsh, M. Dunstan, R. Scannell, and F. Serra, Rev. Sci. Instrum. **81**, 10D521 (2010).
[11] S. Shibaev, G. Naylor, R. Scannell, G. McArdle, T. O'Gorman, and M. J. Walsh, "Control and acquisition for MAST Thomson scattering diagnostics," Fusion Eng. Des. (to be published).